Towards Near-Field Communications for 6G: Challenges and Opportunities

LIU Mengyu[1], ZHANG Yang[1], JIN Yasheng[1], ZHI Kangda[2], PAN Cunhua[1]
(1. Southeast University, Nanjing 210096, China;
2. Queen Mary University of London, London E1 4NS, UK)

DOI: 10.12142/ZTECOM.202401002
https: //kns.cnki.net/kcms/detail/34.1294.TN.20240229.1113.002.html, published online March 1, 2024
Manuscript received: 2023-11-30

Abstract: Extremely large-scale multiple-input multiple-output (XL-MIMO) and terahertz (THz) communications are pivotal candidate technologies for supporting the development of 6G mobile networks. However, these techniques invalidate the common assumptions of far-field plane waves and introduce many new properties. To accurately understand the performance of these new techniques, spherical wave modeling of near-field communications needs to be applied for future research. Hence, the investigation of near-field communication holds significant importance for the advancement of 6G, which brings many new and open research challenges in contrast to conventional far-field communication. In this paper, we first formulate a general model of the near-field channel and discuss the influence of spatial nonstationary properties on the near-field channel modeling. Subsequently, we discuss the challenges encountered in the near field in terms of beam training, localization, and transmission scheme design, respectively. Finally, we point out some promising research directions for near-field communications.

Keywords: near-field communications; extremely large-scale antenna arrays; spatial non-stationarity; beam training; localization

Citation (Format 1): LIU M Y, ZHANG Y, JIN Y S, et al. Towards near-field communications for 6G: challenges and opportunities [J]. ZTE Communications, 2024, 22(1): 3 - 15. DOI: 10.12142/ZTECOM.202401002
Citation (Format 2): M. Y. Liu, Y. Zhang, Y. S. Jin, et al., "Towards near-field communications for 6G: challenges and opportunities," *ZTE Communications*, vol. 22, no. 1, pp. 3 - 15, Mar. 2024. doi: 10.12142/ZTECOM.202401002.

1 Introduction

The advent of the 5G wireless network marks the inception of an era characterized by high speed, low latency, and robust connectivity[1-4]. Millimeter waves (mmWave) and various key technologies like massive multiple-input multiple-output (MIMO) have contributed significantly to the success of 5G, particularly in areas such as smart cities and the Internet of Things (IoT)[5-7]. Although 5G has achieved remarkable results, it still faces limitations in addressing diverse and complex business scenarios, including virtual reality, driverless vehicles and metaverse[8]. These emerging scenarios impose greater demands on the network capacity, prompting researchers to explore 6G wireless networks, which will further surpass the limits of the current technologies to meet much more complex communication needs[9].

In contrast to 5G, 6G has the potential to deliver higher communication rates, ultra-reliable and low latency communications (URLLC), and ubiquitous coverage[10-11]. In order to achieve these goals for 6G, some technologies considered promising for 6G have attracted significant attention, such as extremely large-scale MIMO (XL-MIMO) and Terahertz (THz) communications[12]. Specifically, XL-MIMO can realize ultra-high network throughput and support a large number of users by further increasing the number of antennas on massive MIMO. Meanwhile, emerging technologies like reconfigurable intelligent surface (RIS) and artificial intelligence (AI) techniques empower XL-MIMO to attain increased spectral efficiency, enhanced positioning accuracy, and broader network coverage across a more diverse frequency range. Also, THz communications, with its capacity to exploit richer spectrum resources for enhanced data transmission rates, is a key candidate spectrum technology with significant potential.

However, the new technologies in 6G, e.g., THz communications and XL-MIMO, also lead to operating frequency band escalation and antenna array aperture expansion. As a result, Rayleigh distance, the crucial parameter, that distinguishes between the near-field and far-field boundaries of electromagnetic (EM) wave propagation changes significantly[12]. For example, Ref. [13] gave the Rayleigh distances corresponding to different array apertures, where the near-field range corresponding to an array of 0.5 m aperture was already as high as

This work was supported in part by National Key Research and Development Young Scientist Project 2023YFB2905100, the National Natural Science Foundation of China under Grant Nos. 62201137 and 62331023, the Fundamental Research Funds for the Central Universities under Grant No. 2242022k60001, and the Research Fund of National Mobile Communications Research Laboratory, Southeast University, China under Grant No. 2023A03.

47 m for millimeter waves at 28 GHz. As the Rayleigh distance increases, the user will be easily located in the near field rather than the far field of the base station (BS), meaning that the consideration of the near-field effect is crucial in 6G wireless communications. Within the near field, far field models that approximate EM waves as plane waves are no longer accurate and the spherical shaping of the wavefront cannot be neglected[14]. This new property renders current wireless communication models and findings based on far field assumptions inapplicable in the near-field cases. Therefore, it is necessary to re-investigate the challenges, potential benefits, and solutions introduced by considering near-field communications to advance 6G communication capabilities.

Nowadays, there are relatively few articles about near-field communication in 6G[15-18]. The author of Ref. [15] provided an overview of 6G wireless systems including challenges, insights, and related opportunities. Although the article elaborated on the challenges brought by the near field in future 6G wireless communication, there is a lack of explanation of its specific issues and opportunities. The authors of Ref. [16] presented an overview of near-field communications, contrasted it with far-field communications, and analyzed the key challenges. However, the description of the channel modeling process is neglected. The authors of Ref. [17] studied the basic channel models, antenna structures, and analytical foundations. Furthermore, the authors of Ref. [18] studied the new opportunities brought by the near-field beam focusing caused by the near-field communications, which is different from that in the far field. Different from the above articles, we focus on more specific research problems in near-field communications, especially the combination of near-field communication and new technologies, including the latest research results in the fields of deep learning and near-field beam training, RIS-aided near-field localization, and near-field transmission scheme design with visibility regions (VRs).

In this paper, we systematically present the fundamental models, recent advancements, and solutions in 6G near-field communication. To begin with, we introduce the overall spatial channel model, where the communication region is divided into three parts given different characteristics of array propagation signal phases and power. Subsequently, we introduce the formulation of the channel model encompassing the MIMO systems, accounting for both the far field and the near field. Then, we present recent advances in near-field communication for 6G, including near-field beam training, near-field localization, and near-field transmission scheme design. We elaborate on the challenges encountered in near-field communication within these use cases and provide corresponding solutions. Finally, we share some promising research directions for near-field communication, such as investigating the effectiveness of near-field beam training in complex environments, proposing near-field localization algorithms with low complexity and overhead, and carrying out channel measurements to verify and modify the near-field EM channel model.

2 Fundamentals of Near-Field Communications

In this section, we first introduce the overall space channel model. Subsequently, we elaborate on the modeling approach to the near-field channel. Additionally, the spatial nonstationary property of the channel in the near field is investigated.

2.1 Analysis of the Overall Space Channel Model

As illustrated in Fig. 1, the space from BS to the user can be divided into three regions: far field, radiating near field, and reactive near field. These regions are divided according to the Rayleigh distance and Fresnel distance[19-21], respectively. The far field refers to the region where the distance between the transmitter and the receiver exceeds the Rayleigh distance, allowing the propagating signal to be safely approximated as the plane wave. In the radiating near field, the distance between the transmitter and the receiver is typically less than the Rayleigh distance but greater than the Fresnel distance, where the propagating signal can no longer be modeled as the plane wave; instead, the accurate spherical wave model

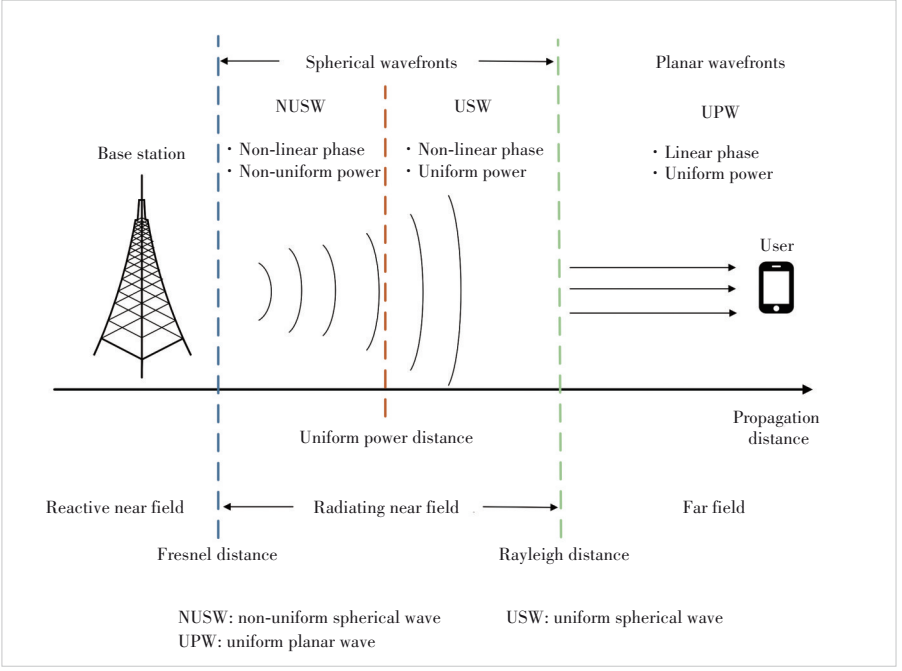

▲Figure 1. Overall channel model

should be utilized. In the reactive near field where the EM fields are reactive, signals are not propagated as EM waves but stored or released as energy. Since the distance of the reactive near field is very small, the near field in the following discussion mainly refers to the radiating near field.

Additionally, as depicted in Fig. 1, we categorize the far and near fields into three models[17]. 1) Uniform planar wave (UPW): in the far field, signal propagation typically conforms to this model where the phase difference in signal transmission is linear and the transmitted power is uniform for different antenna elements. 2) Uniform spherical wave (USW): in the near field, when the distance between the transmitter and receiver is less than the Rayleigh distance but greater than the uniform power distance[17, 22], the phase difference between the signals propagated by different antennas is nonlinear while the transmitted power is uniform. 3) Non-uniform spherical wave (NUSW): in the near field, when the distance between the transmitter and the receiver is less than the uniform power distance, the phase difference between the signals propagated by different antennas is nonlinear and the transmitted power is not uniform.

2.2 Generic Channel Modeling

In this section, we first derive a general channel model considering MIMO systems. After that, we analyze a simple scenario of a multiple-input single-output (MISO) system with a uniform linear array (ULA) array at the base station to gain more insights.

2.2.1 MIMO Channel Model

As shown in Fig. 2, we first analyze the channel model of the MIMO system. Let us consider a MIMO system that includes a transmitter with N_t antennas and user equipment (UE) with N_r antennas. We first set the center of the BS antenna as the origin, i.e., $\boldsymbol{s}_0 = [0,0,0]^{\mathrm{T}}$. Then, the locations of the m-th element of BS and the n-th antenna of UE can be expressed by $\boldsymbol{s}_m = [s_x^m, s_y^m, s_z^m]^{\mathrm{T}}, \forall m = -(N_t-1)/2, \cdots, (N_t-1)/2$ and $\boldsymbol{u}_n = [u_x^n, u_y^n, u_z^n]^{\mathrm{T}}, \forall n = -(N_r-1)/2, \cdots, (N_r-1)/2$, respectively. In addition, the distance between the m-th antenna of UE and the n-th element of BS is given by $r_{m,n} = \left\| \boldsymbol{u}_n - \boldsymbol{s}_m \right\|$. Then, the line-of-sight (LoS) channel coefficient can be expressed as:

$$\left[\boldsymbol{H}_{\mathrm{LoS}}\right]_{m,n} = \alpha_{m,n} e^{-j\frac{2\pi}{\lambda} r_{m,n}}, \tag{1}$$

where $\alpha_{m,n}$ represents the amplitude for the channel link between the m-th antenna of BS and the n-th element of UE.

1) Far-field channel

Firstly, we can define the propagation direction vector from the transmitter to UE as follows:

$$\boldsymbol{v}(\theta,\phi) = [\cos\theta\sin\phi, \sin\theta\sin\phi, \cos\phi]^{\mathrm{T}}. \tag{2}$$

Based on the plane-wave assumption[23] for the far-field channel, the propagation distance can be approximated by $r_{m,n} \approx r_0 - \boldsymbol{v}^{\mathrm{T}}(\theta,\phi)\boldsymbol{s}_m - \boldsymbol{v}^{\mathrm{T}}(\theta,\phi)\left(\boldsymbol{u}_n - \boldsymbol{u}_0\right)$, where $r_0 = \left\| \boldsymbol{u}_0 - \boldsymbol{s}_0 \right\|$ denotes the distance between the central elements of the receiving and the transmitting antenna arrays. Moreover, we assume $\alpha_{m,n} \approx \alpha$, where α denotes the amplitude for the channel link between the central antenna elements of the transmitter and the UE. Then, the LoS far-field channel coefficient can be rewritten as:

$$\left[\boldsymbol{H}_{\mathrm{LoS}}^{\mathrm{far}}\right]_{m,n} = \alpha_{m,n} e^{-j\frac{2\pi}{\lambda} r_{m,n}} \approx \alpha e^{-j\frac{2\pi}{\lambda} r_0} e^{j\frac{2\pi}{\lambda}\boldsymbol{v}^{\mathrm{T}}(\theta,\phi)\boldsymbol{s}_m} e^{j\frac{2\pi}{\lambda}\boldsymbol{v}^{\mathrm{T}}(\theta,\phi)\left(\boldsymbol{u}_n - \boldsymbol{u}_0\right)}. \tag{3}$$

From the channel coefficients in Eq. (3), we can decouple the MIMO channel into the product of two array response vectors. Therefore, the far-field LoS MIMO channel can be expressed as:

$$\boldsymbol{H}_{\mathrm{LoS}}^{\mathrm{far}} = \alpha \boldsymbol{a}_{\mathrm{far}}^{\mathrm{UE}}(\theta,\varphi)\left(\boldsymbol{a}_{\mathrm{far}}^{\mathrm{TR}}(\theta,\varphi)\right)^{\mathrm{T}}, \tag{4}$$

where

$$\boldsymbol{a}_{\mathrm{far}}^{\mathrm{UE}}(\theta,\varphi) = \left[e^{j\frac{2\pi}{\lambda}\boldsymbol{v}^{\mathrm{T}}(\theta,\phi)\left(\boldsymbol{u}_{-(N_r-1)/2} - \boldsymbol{u}_0\right)}, \cdots, e^{j\frac{2\pi}{\lambda}\boldsymbol{v}^{\mathrm{T}}(\theta,\phi)\left(\boldsymbol{u}_{(N_r-1)/2} - \boldsymbol{u}_0\right)}\right]^{\mathrm{T}}, \tag{5}$$

$$\boldsymbol{a}_{\mathrm{far}}^{\mathrm{TR}}(\theta,\varphi) = \left[e^{j\frac{2\pi}{\lambda}\boldsymbol{v}^{\mathrm{T}}(\theta,\phi)\boldsymbol{s}_{-(N_t-1)/2}}, \cdots, e^{j\frac{2\pi}{\lambda}\boldsymbol{v}^{\mathrm{T}}(\theta,\phi)\boldsymbol{s}_{(N_t-1)/2}}\right]^{\mathrm{T}}. \tag{6}$$

Furthermore, the form of the far-field non-line-of-sight (NLoS) channel is similar to the far-field LoS channel. Therefore, the overall far-field MIMO channel model with multi-path components is given by:

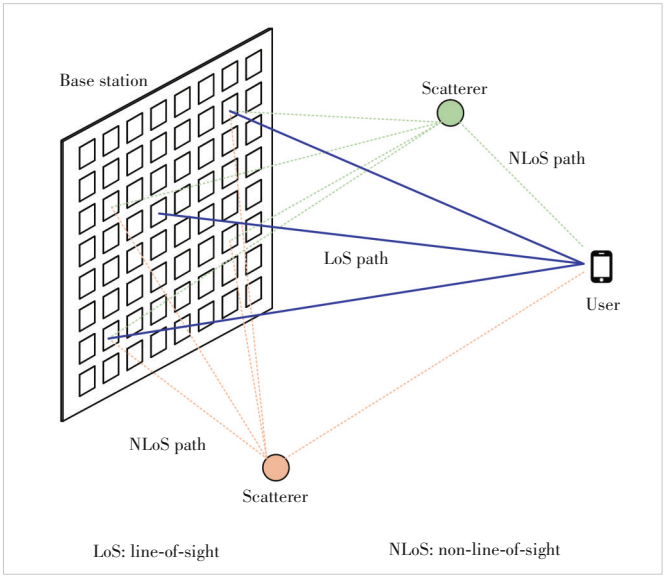

▲Figure 2. Near-field channel model

$$\boldsymbol{H}^{\text{far}} = \alpha \boldsymbol{a}_{\text{far}}^{\text{UE}}(\theta,\varphi)(\boldsymbol{a}_{\text{far}}^{\text{TR}}(\theta,\varphi))^{\text{T}} + \sum_{l=1}^{L} \beta_l \boldsymbol{a}_{\text{far}}^{\text{UE}}(\theta_l,\varphi_l)(\boldsymbol{a}_{\text{far}}^{\text{TR}}(\theta_l,\varphi_l))^{\text{T}}. \tag{7}$$

2) Near-field channel

As shown in Fig. 2, the NLoS channels in the near field exist between the transmitter and the UE due to the presence of scatterers. Clearly, the NLoS channel can be divided into the combination of two MISO channels, i.e., the channel from the UE to the scatterer and the channel from the scatterer to the transmitter. Therefore, the NLoS channel can be decoupled as the product of two array response vectors:

$$\boldsymbol{H}_{\text{NLoS}}^{\text{near}} = \sum_{l=1}^{L} \beta_l \boldsymbol{a}_{\text{near}}^{\text{UE}}(\boldsymbol{r}_l)(\boldsymbol{a}_{\text{near}}^{\text{TR}}(\boldsymbol{r}_l))^{\text{T}}, \tag{8}$$

where β_l and $\mathbf{r}_l$ denote the channel coefficients for the l-th NLoS path and the location of the l-th scatterer, respectively. And the near-field array response vector $\boldsymbol{a}_{\text{near}}^{\text{UE}}(\boldsymbol{r}_l)$ and $\boldsymbol{a}_{\text{near}}^{\text{TR}}(\boldsymbol{r}_l)$ can be given by:

$$\boldsymbol{a}_{\text{near}}^{\text{UE}}(\boldsymbol{r}_l) = \left[e^{-j\frac{2\pi}{\lambda}\left\|\boldsymbol{u}_{-(N_r-1)/2}-\boldsymbol{r}_l\right\|}, \cdots, e^{-j\frac{2\pi}{\lambda}\left\|\boldsymbol{u}_{(N_r-1)/2}-\boldsymbol{r}_l\right\|} \right]^{\text{T}}, \tag{9}$$

$$\boldsymbol{a}_{\text{near}}^{\text{TR}}(\boldsymbol{r}_l) = \left[e^{-j\frac{2\pi}{\lambda}\left\|\boldsymbol{s}_{-(N_t-1)/2}-\boldsymbol{r}_l\right\|}, \cdots, e^{-j\frac{2\pi}{\lambda}\left\|\boldsymbol{s}_{-(N_t-1)/2}-\boldsymbol{r}_l\right\|} \right]^{\text{T}}. \tag{10}$$

However, the LoS channel in the near field cannot be decoupled as the product of two array response vectors. Specifically, the LoS channel coefficient can be expressed as:

$$\left[\boldsymbol{H}_{\text{LoS}}^{\text{near}}\right]_{m,n} = \alpha_{m,n} e^{-j\frac{2\pi}{\lambda}r_{m,n}} = \alpha_{m,n} e^{-j\frac{2\pi}{\lambda}\left\|\boldsymbol{u}_n-\boldsymbol{s}_m\right\|}. \tag{11}$$

Therefore, the overall near-field channel with multi-path components can be modeled as

$$\boldsymbol{H}^{\text{near}} = \boldsymbol{H}_{\text{LoS}}^{\text{near}} + \sum_{l=1}^{L} \beta_l \boldsymbol{a}_{\text{near}}^{\text{UE}}(\boldsymbol{r}_l)(\boldsymbol{a}_{\text{near}}^{\text{TR}}(\boldsymbol{r}_l))^{\text{T}}. \tag{12}$$

2.2.2 MISO Channel Model Based on ULA Base Station

To more intuitively understand the properties of the near-field channel, we next simplify it to the uniform linear array (ULA) model.

We assume that the base station is equipped with N_t-ULA antennas and the user is equipped with a single antenna. In the case of ULA, we can ignore the z-axis and assume the locations of the m-th antenna element of BS and UE as $\boldsymbol{u} = [r_0\cos\theta, r_0\sin\theta]^{\text{T}}$ and $\boldsymbol{s}_m = [md, 0]^{\text{T}}, \forall m = -(N_t-1)/2, \cdots, (N_t-1)/2$, respectively, where d denotes spacing between two adjacent antenna elements. Therefore, the distance between the m-th antenna element of the transmitter and UE can be expressed as:

$$r_m = \left\|\boldsymbol{u}-\boldsymbol{s}_m\right\| = \sqrt{r_0^2 - 2r_0 md\cos\theta + m^2d^2} \overset{(a)}{\approx} r_0 - md\cos\theta + \frac{m^2d^2\sin^2\theta}{2r_0}. \tag{13}$$

where (a) denotes the Taylor expansion approximation, which is also called the Fresnel approximation[24]. Then, the near-field array response vector for the ULA channel is given by

$$\boldsymbol{a}_{\text{ULA}}^{\text{near}}(\theta) = \left[e^{j\frac{2\pi}{\lambda}\left(-(N_t-1)/2)d\cos\theta - \frac{(-(N_t-1)/2)^2d^2\sin^2\theta}{2r}\right)}, \cdots, e^{j\frac{2\pi}{\lambda}\left((N_t-1)/2)d\cos\theta - \frac{((N_t-1)/2)^2d^2\sin^2\theta}{2r}\right)} \right]^{\text{T}}. \tag{14}$$

For the far-field scenario, the distance r_m can be approximated as $r_m = r_0 - md\cos\theta$. Based on this, the far-field array response vector for the ULA channel can be expressed by:

$$\boldsymbol{a}_{\text{ULA}}^{\text{far}}(\theta) = \left[e^{-j\frac{2\pi}{\lambda}(-(N_t-1)/2)d\cos\theta}, \cdots, e^{-j\frac{2\pi}{\lambda}(N_t-1)/2)d\cos\theta} \right]^{\text{T}}. \tag{15}$$

Clearly, it can be observed from Eq. (14) that the phase of the near-field array response vector is not a linear function of m. However, for the far-field array response vector in Eq. (15), the phase is a linear function of m.

From the above derivation, it is evident that the far-field plane wave assumption will result in an obvious error in the practical near-field scenario. Moreover, the array response vectors in the near-field channel are more complex, posing challenges to conventional transmission scheme design and channel estimation.

2.3 Near-Field Channel with Spatial Non-Stationarity Property

In the near-field scenario, since the size of the transmitter's antenna array is significantly increased, spatial non-stationary properties[25-26] start to appear. Consequently, we introduce the concept of spatial non-stationarities and VRs based on the modeling of the near-field channel.

As illustrated in Fig. 3, spatial non-stationarities mean that due to the large array aperture, different parts of the antenna array could have different views of the propagation environment. This property restricts the user to receiving only a portion of the signal transmitted by the antenna array, which is referred to as VR of the user. The VRs are formed primarily due to two reasons as follows[12]. 1) Unequal path loss: Based on the near-field channel, the increase in antenna array size makes it impossible to ignore the difference in path loss from different array elements to the user. Some of the array elements that are farther away from the user suf-

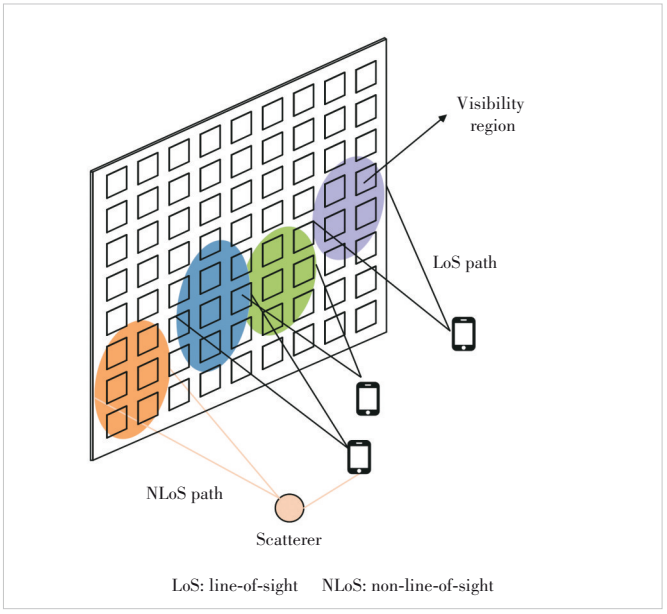

▲Figure 3. Illustration of spatial non-stationary property

fer greater path loss. As a result, most of the power of the signal received by the user comes from those array elements with lower path loss. This phenomenon leads to the appearance of VRs. 2) Blockage: The large antenna size increases the possibility of obstacles between the user and some antennas. This obstruction prevents the user from receiving signals from some sub-arrays which are blocked by obstacles, bringing the emergence of VRs.

Then, we can obtain the near-field channel considering the VRs[27 - 28]:

$$\boldsymbol{h}^{\text{near}} = \alpha e^{-j\frac{2\pi}{\lambda}r}\boldsymbol{a}^{\text{near}}(\boldsymbol{r})\odot\boldsymbol{f}(\boldsymbol{\Phi}) + \sum_{l=1}^{L}\beta_l\boldsymbol{a}^{\text{near}}(\boldsymbol{r}_l)\odot\boldsymbol{f}(\boldsymbol{\Phi}_l), \tag{16}$$

where $\boldsymbol{\Phi}$ and $\boldsymbol{\Phi}_l$ represent the index of the array that is visible to the user and the l-th scatterer, respectively, and $\boldsymbol{f}(\boldsymbol{\Phi})$ denotes the vector of VRs, which is given by:

$$[\boldsymbol{f}(\boldsymbol{\Phi})]_n = \begin{cases} 1, n \in \boldsymbol{\Phi}, \\ 0, n \notin \boldsymbol{\Phi}. \end{cases} \tag{17}$$

Moreover, when the prior information about the actual environment is unknown, the user's VR information can be modeled as a Markov process or birth and death process[29 - 30].

3 Challenges and Research Progress in Near-Field Communications

In this section, we will present some challenging directions in near-field communication, including beam training, localization and transmission scheme design. For each challenge, we then provide a detailed literature review and the latest research progress.

3.1 Beam Training for Near-Field Communications

3.1.1 Challenges

Codebook-based beam training intends to identify the optimal combination of transmitting and receiving beams for subsequent data transmission. Most of the existing research on beam training has been conducted under the assumption of far field[31 - 34]. However, for next-generation communication systems, the use of XL-MIMO techniques invalidates existing far-field assumptions, making it inevitable to consider the near-field model[14]. The change from far-field to near-field presents opportunities and challenges to beam training.

In the far-field domain, the codebook design only considers the angle domain information as shown in Fig. 4(a), where the angles are uniformly sampled. However, the Rayleigh distance that distinguishes the near field from the far field expands with the growth of the antenna array, necessitating the consideration of near-field effects[20]. Unlike the far field, the distance information is added in the near-field domain codebook design, making the codebook dimension dramatically higher[17]. Therefore, it becomes crucial to investigate codebook-based beam training methods under the near-field domain to reduce overhead.

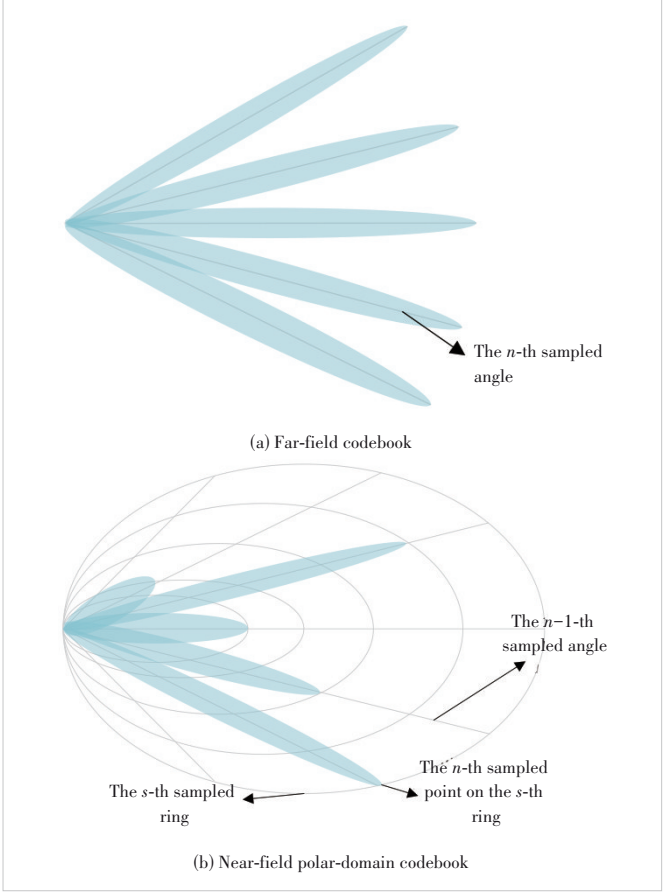

▲Figure 4. Codebook for the far field and near field

3.1.2 Existing Works

Similar to far-field beam training, near-field beam training can be accomplished using both traditional and machine learning-based methods, with beam sweeping and hierarchical beam training[35].

The most straightforward way for codebook-based near-field beam training is beam sweeping; however, this approach introduces unacceptable pilot overhead due to the expansion of the codebook dimension. To tackle this problem, researchers designed a hierarchical beam training scheme based on a hierarchical near-field codebook, which reduces the pilot overhead[36]. Furthermore, the authors of Ref. [24] designed a polar-domain near-field codebook in which the angular domain was uniformly sampled while the distance was sampled as inhomogeneous distance rings as shown in Fig. 4(b). By utilizing the polar-domain near-field codebook, the authors in Ref. [37] proposed a new two-phase beam training method. Specifically, beam training is accomplished by angular domain sweeping based on a far-field codebook and distance sweeping based on a polar-domain near-field codebook, respectively, which significantly reduces the training overheads. Nevertheless, the necessary pilot overhead remains excessive, and the impact of noise on the hierarchical beam training scheme cannot be neglected. Deep learning constitutes a subdivision of machine learning that relies on artificial neural networks to emulate and acquire intricate data representations and features through multi-layer neural network architectures. It gradually abstracts high-level features and representations in the input data through multi-layer nonlinear transformations to enable learning and reasoning about complex tasks. Recently, deep learning has been widely used in wireless communication to reduce the cost of beam training[34, 38 – 41]. The authors of Ref. [34] took the received signals corresponding to a few beams as the input for deep neural networks (DNN) to estimate the beam that best matches the channel. Ref. [34] introduced a DNN-based method with location information to reduce beam training overhead. Inspired by the above work, the authors of Refs. [38 – 41] have extended the deep learning method to near-field beam training. The authors of Ref. [38] used a part of the near-field beam as the input of DNN for prediction. By contrast, Ref. [40] utilized the information of far-field wide beam as the input of the deep learning network to predict the optimal beam to reduce the overhead. In the following part, we present more details of the research work in Ref. [40].

3.1.3 Near-Field Beam Training Based on Deep Learning

A well-trained deep learning approach is used in Ref. [40] to uncover the angle and distance information carried by the far-field wide beam to find the optimal near-field codeword. Specifically, the authors constructed the neural network structure shown in Fig. 5 for the angle and distance domains, respectively. The deep learning-based near-field beam training problem can be formulated as:

$$n^* = f_1(\boldsymbol{y}^{\boldsymbol{w}}), n^* \in \{1,2,\cdots,N\}, \tag{18}$$

$$s^* = f_2(\boldsymbol{y}^{\boldsymbol{w}}), s^* \in \{1,2,\cdots,S\}, \tag{19}$$

where $\boldsymbol{y}^{\boldsymbol{w}}$ is received signals of the far-field wide beams. n^* and s^* denote the optimal angle and ring indices in the polar domain, respectively.

The input of the neural network is the real and imaginary part of $\boldsymbol{y}^{\boldsymbol{w}}$, which is transformed into a matrix form, respectively. Then with carefully designed convolutional and fully connected layers, the final output can be written as:

$$\hat{\boldsymbol{P}}^a = \left[\hat{p}_1^a, \hat{p}_2^a, \cdots, \hat{p}_N^a\right]^{\mathrm{T}}, \hat{\boldsymbol{P}}^r = \left[\hat{p}_1^r, \hat{p}_2^r, \cdots, \hat{p}_S^r\right]^{\mathrm{T}}, \tag{20}$$

where $\hat{p}_n^a$ and $\hat{p}_s^r$ denote the estimated probability of the optimal angle and ring indices, respectively. The authors determine the index corresponding to the angle and distance under the polar-domain codebook by finding the maximum estimated probability in $\hat{\boldsymbol{P}}^a$ and $\hat{\boldsymbol{P}}^r$ to achieve the optimal beam. In addition, the authors offer an improved scheme, in which it performs additional tests by obtaining K maximum possible angle indices and L maximum possible distance indices in $\hat{\boldsymbol{P}}^a$ and $\hat{\boldsymbol{P}}^r$. It can be formulated as:

$$\left\{\hat{p}_{\sigma_1}^{\mathrm{a}}, \hat{p}_{\sigma_2}^{\mathrm{a}}, \cdots, \hat{p}_{\sigma_K}^{\mathrm{a}}\right\} = \left\langle\left\{\hat{p}_1^{\mathrm{a}}, \hat{p}_2^{\mathrm{a}}, \cdots, \hat{p}_N^{\mathrm{a}}\right\}\right\rangle, \left\{\hat{p}_{\gamma_1}^{\mathrm{r}}, \hat{p}_{\gamma_2}^{\mathrm{r}}, \cdots, \hat{p}_{\gamma_S}^{\mathrm{T}}\right\} = \left\langle\left\{\hat{p}_1^{\mathrm{r}}, \hat{p}_2^{\mathrm{T}}, \cdots, \hat{p}_S^{\mathrm{r}}\right\}\right\rangle, \tag{21}$$

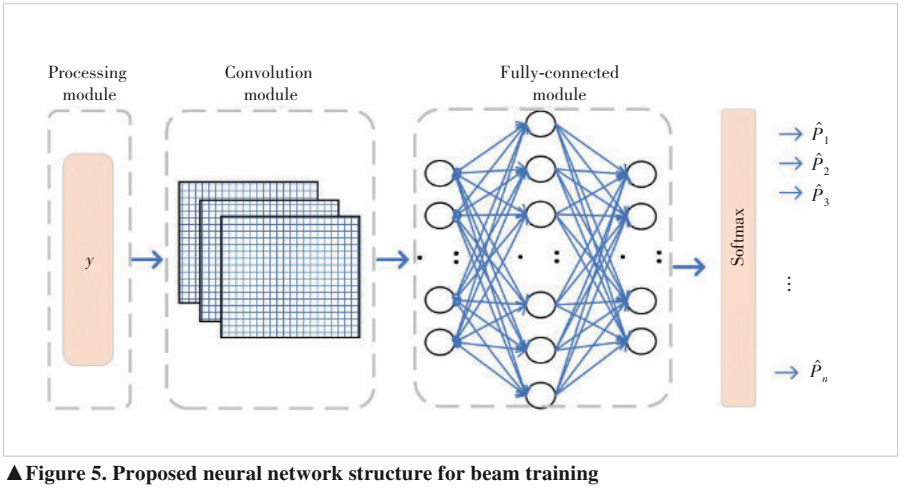

▲Figure 5. Proposed neural network structure for beam training

$$\mathcal{L}_a = \{\sigma_1,\sigma_2,\cdots,\sigma_K\}, \mathcal{L}_d = \{\gamma_1,\gamma_2,\cdots,\gamma_L\}, \quad (22)$$

where $\langle . \rangle$ denotes the order operation. By performing KL additional near-field beam training tests, we can get the optimal near-field beam.

Simulation results validate the advantages of original and improved schemes compared with the sweep scheme as shown in Fig. 6. The improved scheme can achieve over 90% of the data rate and reduce overhead by 95% compared with the sweep scheme. This stems from the remarkable data processing capabilities in neural networks and the full leveraging of the output in the improved scheme.

3.2 Localization for Near-Field Communications

3.2.1 Challenges

In THz systems, the performance of positioning can be improved since all the geometric information is included in the channel state information (CSI) measurements, which can be estimated more accurately with narrow beams[42]. In addition, RIS can provide reliable and high-precision estimation performance with low energy consumption, and the large size of the RIS panel enables high-accuracy positioning parameter estimation[43]. Therefore, research on RIS-aided localization has attracted increasing attention, while most of them adopted the planar wavefront based on the far-field channel model[44 - 52].

However, in some envisioned scenarios with the XL-RIS panel, the typical indoor communication distances may not guarantee the validity of far-field conditions. In addition, UE is usually located in the near-field area of the XL-RIS in the THz localization system owing to the short wavelength[53]. Therefore, the spherical wavefront of near-field transmission should be considered in XL-RIS-based THz localization, where the transmitted wavefront will arrive at each element of the RIS panel with different Angles of Arrival (AoAs). The assumption that all the RIS elements share a common AoA of the same path is no longer valid, making the channel estimation and localization more challenging.

3.2.2 Existing Works

Although near-field RIS behavior has attracted increasing attention recently, the study on RIS-aided near-field localization is still in its infancy. Most researchers considering the spherical wavefront mainly analyzed the Fisher information matrix (FIM) and the Cramer-Rao lower bound (CRLB) to illustrate the position error bound (PEB) and orientation error bound (OEB), which could be derived as performance benchmarks for the practical algorithms[48, 54 - 55]. In addition, the authors of Ref. [56] proposed an algorithm of RIS-aided near-field joint channel estimation and localization (NF-JCEL) in THz systems, which addressed the specific issue of channel estimation and UE positioning in the near-field scenario.

3.2.3 RIS-Aided Near-Field Localization Algorithm

The authors of Ref. [56] considered the uplink transmission of a THz localization system as shown in Fig. 7, where the direct links between the AP and the UE are assumed to be obstructed. The receiving antenna arrays of the AP and the RIS are assumed to be ULA and UPA, respectively.

Assuming that the UE is located at the near field of the RIS panel, the authors derived the two-dimensional Fresnel approximation of the distance between the m-th element and UE u, and approximated the near-field array response as:

$$\boldsymbol{a}_{R,u}^{N,i}(\omega_u,\varphi_u,d_u^0)[m] = \exp\left(-j\frac{2\pi}{\lambda_i}\left(J_m(\omega_u,\varphi_u) + Q_m(\omega_u,\varphi_u,d_u^0)\right)\right), \quad (23)$$

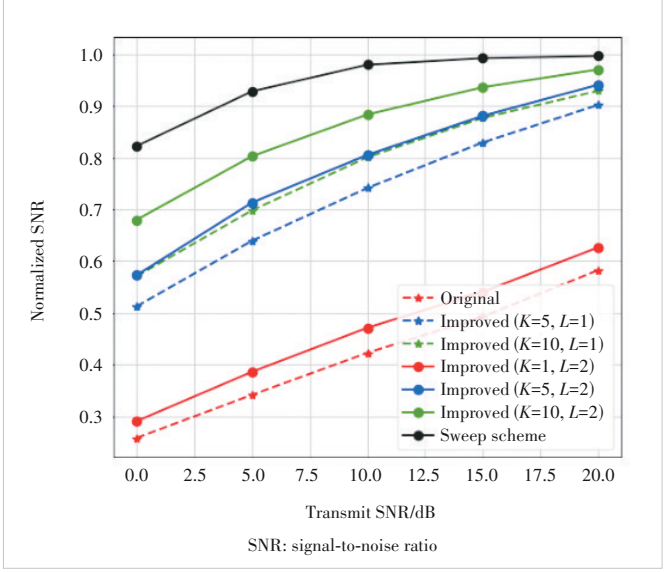

▲Figure 6. Normalized SNR for the original and improved schemes

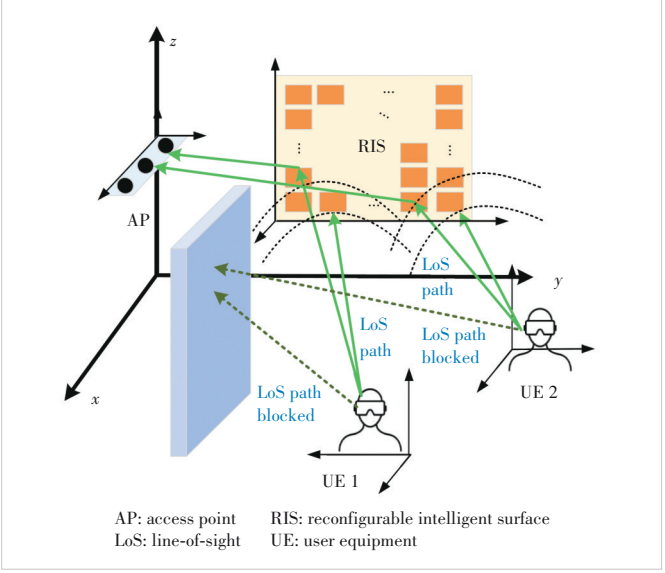

▲Figure 7. System model and communication scenario

where $J_m(\omega_u,\varphi_u)=m_z\Delta_R\omega_u-m_y\Delta_R\varphi_u$, and $Q_m(\omega_u,\varphi_u,d_u^0)=\left((m_z\Delta_R)^2+(m_y\Delta_R)^2-J_m^2(\omega_u,\varphi_u)\right)/2d_u^0$.

Then, the authors carried out the NF-JCEL algorithm by estimating the AoAs $\omega_u=\sin\phi_{u,0}$, $\varphi_u=\sin\theta_{u,0}\cos\phi_{u,0}$, the distance d_u^0, and the cascaded channel attenuation $g_{u,i}$, and finally obtained the position of UE u by utilizing the geometric relationship. Furthermore, because the steering vectors were frequency-dependent, the authors processed the channel estimation on each sub-band.

1) RIS training phase shifts and pilot design

The authors utilized different RIS phase shift vectors to obtain a unique estimation of the channel matrix. The pseudo-random (PN) sequences were utilized as the transmitting pilot at different time slots, which are statistically orthogonal with each other, and the RIS phase shift vector changed for S times in a pilot data duration. Then the composited signal vector which collected the received signals in the S different phase shifts could be obtained, and we had a least square (LS) estimator of $\boldsymbol{A}\boldsymbol{x}_t$ as $\overline{\boldsymbol{A}\boldsymbol{x}}_t$, where $\boldsymbol{A}$ is the channel matrix to be estimated, and $\boldsymbol{x}_t$ is the pilot sequence in the t-th time slot.

Note that the rank of the cascaded channel moves up by employing diverse phase shifts of the RIS to avoid noise amplification when utilizing the LS estimation. Since the channel coefficients are unknown, the existing RIS phase designs such as the random phase shift and the Discrete Fourier Transform (DFT) matrix are considered. By collecting the received signal in the τ pilot durations, the covariance matrix of the received signal is estimated as the mean covariance matrix of $\overline{\boldsymbol{A}\boldsymbol{x}}_t$.

2) Estimation of AoAs

The authors provided a novel method to separate the distance and AoAs in the covariance matrix. With complicated mathematical manipulations, they constructed a down-sampled Toeplitz matrix $\boldsymbol{T}$ to decouple the distance and the AoAs. Therefore, the far-field angle estimation methods could be obtained with the sampled correlation matrix.

Specifically, the authors applied a computationally efficient subspace-based method to estimate the angles. By leveraging the key idea of the MUSIC algorithm, the AoAs could be estimated by minimizing the following cost function:

$$f(\omega,\varphi)=\boldsymbol{b}^{\mathrm{H}}(\omega,\varphi)\boldsymbol{\Pi}_m\boldsymbol{b}(\omega,\varphi), \tag{24}$$

where $\boldsymbol{b}(\omega,\varphi)=\boldsymbol{v}(\omega)\otimes\boldsymbol{s}(\varphi)$, $\boldsymbol{v}(\omega)_{[z]}=\exp\left(-j\frac{4\pi}{\lambda}z\Delta_R\omega\right)$, $\boldsymbol{s}(\varphi)_{[y]}=\exp\left(-j\frac{4\pi}{\lambda}y\Delta_R\varphi\right)$, and $\boldsymbol{\Pi}_m$ is designed by utilizing the property of the sampled correlation matrix $\boldsymbol{T}$.

By applying the Lagrangian multiplier method, the relationship between each optimal ω_u and φ_u is obtained. Then, substitute the equation into the objective function and the optimal value of ω can be reached by solving a one-dimensional problem. Since $\omega_u=\sin\phi_u$, we can search in the interval of $\omega_u\in[-1,1]$ and obtain the U largest peaks as the estimator of ω_u. Finally, by utilizing the relationship between ω_u and φ_u, we have U vectors $\hat{\boldsymbol{s}}(\varphi_u)$ corresponding to $\hat{\omega}_u$, and the estimator of φ_u is obtained by applying the LS estimation.

3) Estimation of distances, channel gains and locations

Similar to the method of tackling ω and φ, the authors transform the estimation of distance into the following problem.

$$d_u^{0\,*}=\arg\min_{d_u^0}\left(\left(\mathrm{diag}\{\boldsymbol{p}_u\}\boldsymbol{q}_u\right)^{\mathrm{H}}\boldsymbol{\Pi}_n\left(\mathrm{diag}\{\boldsymbol{p}_u\}\boldsymbol{q}_u\right)\right), \tag{25}$$

where $\boldsymbol{p}_u=\left[\exp\left(-j\frac{2\pi}{\lambda}J_{-N_0}\right),\cdots,\exp\left(-j\frac{2\pi}{\lambda}J_{N_0}\right)\right]^{\mathrm{T}}$, $\boldsymbol{q}_u=\left[\exp\left(-j\frac{\pi Q_{-N_0}}{\lambda d_u^0}\right),\cdots,\exp\left(-j\frac{\pi Q_{N_0}}{\lambda d_u^0}\right)\right]$, and $\boldsymbol{\Pi}_n$ is designed in the similar way as $\boldsymbol{\Pi}_m$. By conducting one-dimensional search, the U largest peaks of the searching results are obtained as the estimated distances.

Finally, the LS method can be applied to estimate the channel gain of sub-band i, and the localization of UE u can be obtained according to the geometric relationship with the estimation over different frequency bands.

4) Simulation results

Simulation results validate the advantages of the NF-JCEL algorithm over its far-field counterpart in the near-field scenario. As shown in Fig. 8(a), the NF-JCEL algorithm outperforms the corresponding far-field cases in the root mean square error (RMSE) of UE locations. In addition, along with the increase of elements, the NF-JCEL algorithm obtains better performance while the conventional far-field model suffers severe degradation. When it comes to the RMSE performance of the estimated channel coefficients, similar trends in the sum RMSE can be observed in Figs. 8 (b) and 8(c).

This phenomenon is owing to the fact that more elements can provide more angular information, thus leading to higher angular resolution when estimating the AoAs. In contrast, the conventional far-field model neglects the distinction of AoAs at the RIS, so that the approximation error of the planar wavefront becomes more severe though the correlation matrices of larger dimensions are exploited.

3.3 Transmission Scheme Design for Near-Field Communications

3.3.1 Challenges

As the antenna array size increases, the Rayleigh distance significantly extends from a few meters to tens or hundreds of meters[17]. Consequently, the plane wave assumption in the far field becomes invalid. Based on the spherical wave character-

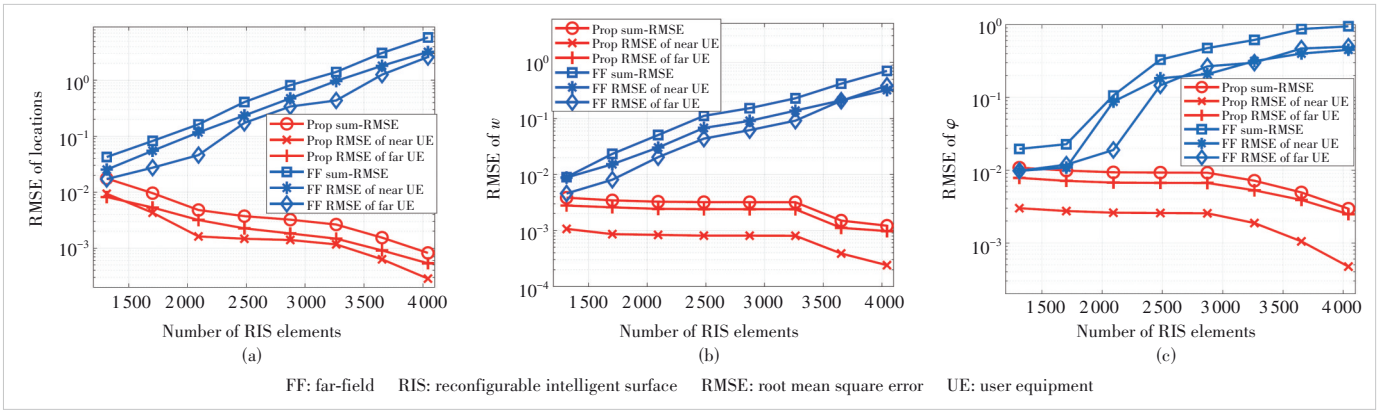

▲**Figure 8. Element number versus RMSE of estimated parameters**

istics, distance information needs to be considered in the near-field channel modeling. Furthermore, with the emergence of large-scale antenna arrays, the dimension of the channel becomes large and the computational complexity for transmission scheme design also greatly increases, which becomes a key design challenge in near-field scenarios. Moreover, the unique spatial non-stationary characteristics in the near field make the performance characteristics and algorithm design different from those in the far field with conventional stationary channels. This necessitates the exploration of more accurate near-field channel models and raises a new challenge: how to design new transmission schemes based on the characteristics of the near-field channel.

3.3.2 Existing Works

The near-field channel introduces several new channel characteristics: the spherical wave property of the propagating signal and the spatial non-stationary property. Recently, some researchers have confirmed the existence of spatial non-stationary properties in near-field channels[26, 57], i.e., the user's transmitted signal may only be received by a small part of the array. Based on this characteristic, the authors of Ref. [26] proposed a channel model based on VRs. To reduce the computational complexity and by exploiting the nature of VRs, the authors of Ref. [58] proposed a graph-based linear receiving algorithm inspired by random access. Moreover, an antenna selection algorithm was proposed in Ref. [59] to improve the total energy efficiency of the system. However, the above work assumes that the VR information is known and the arrays other than the VR receive signal amplitude with values of zero, which is impractical. To fill these gaps, the authors of Ref. [60] first derived a near-field channel model considering antenna polarization based on the EM field theory. Then, a detection algorithm for VRs was proposed, which can obtain VR information of different users. Finally, the authors proposed a linear detection algorithm based on VRs, exploiting VRs information for different users to reduce the computational complexity. In the following part, we present details of the research work in Ref. [60].

3.3.3 Transmission Scheme Design for Near-Field with Spatial Non-Stationaries

The authors of Ref. [60] considered an uplink transmission system with multiple single-antenna users and an XL-MIMO base station, as shown in Fig. 9.

The channel between the (m_x, m_y)-th antenna element of the base station and user k can be expressed as

$$h_{k,m_x,m_y} = \sqrt{\xi_{k,m_x,m_y}}\, e^{-j\chi_{k,m_x,m_y}}, \tag{26}$$

where ξ_{k,m_x,m_y} and χ_{k,m_x,m_y} denote the channel coefficient and phase, respectively.

Then, the authors derive a near-field channel model that takes polarization mismatch into account by using the inhomogeneous Helmholtz wave equation and Green's function. We first define the Δ_x and Δ_y as the antenna spacing along the x-axis and y-axis, respectively. After that, by assuming the location of user k and the (m_x, m_y)-th antenna element as $\boldsymbol{u}_k = [u_{k,x}, u_{k,y}, u_{k,z}]^{\mathrm{T}}$ and $\boldsymbol{p}_{m_x,m_y} = [m\Delta_x, m\Delta_y, 0]^{\mathrm{T}}$, respectively, the channel coefficient and phase are given by:

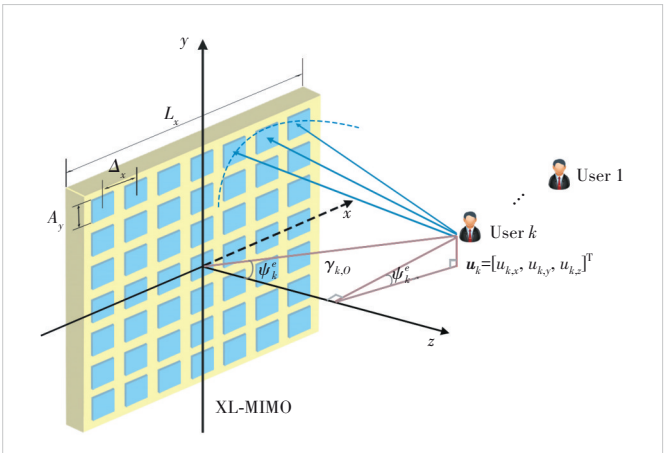

▲**Figure 9. System model in Ref. [60]**

$$\xi_{k,m_x,m_y} \approx \frac{A}{4\pi} \frac{u_{k,z}\left(\left(m_x\Delta_x - u_{k,x}\right)^2 + u_{k,z}^2\right)}{\left\{\left(m_x\Delta_x - u_{k,x}\right)^2 + \left(m_y\Delta_y - u_{k,y}\right)^2 + u_{k,z}^2\right\}^{\frac{5}{2}}}, \quad (27)$$

$$\chi_{k,m_x,m_y} \approx \frac{2\pi}{\lambda}\left\| \boldsymbol{p}_{m_x,m_y} - \boldsymbol{u}_k \right\|. \quad (28)$$

The authors derived an explicit expression for single-user SNR based on the maximum ratio combining (MRC) detector. As shown in Fig. 10(a), the SNR gradually increases to saturation with the increase of antenna numbers. Furthermore, the near-field channel model considering polarization mismatch satisfies the introduced theoretical upper bound.

Next, based on the proposed near-field channel model, the authors proposed a VR-based low-complexity transmission scheme by exploiting the spatial non-stationarity of XL-MIMO. The dimensionality of the channel matrix in the transmission design can be greatly reduced by utilizing this method, thus reducing the computational complexity accordingly. Furthermore, the authors proposed a graph-theory based user grouping algorithm to categorize users with high VRs overlap ratios into one group. The authors then utilized the partial zero-forcing (PZF) detection algorithm to eliminate the mutual interference within each user group, which could further reduce the computational complexity.

As shown in Fig. 10(b), as the number of antenna elements increases, the computational complexity of the whole array (WA)-based design rises considerably. For the VR-based zero-forcing (ZF) algorithm and the graph-theory based PZF algorithm, low computational complexity can be achieved.

4 Future Directions

In this section, several promising directions of near-field communications are discussed according to the contributions and deficiencies of the aforementioned appealing works.

4.1 AI-Aided Near-Field Beam Training

The AI-based near-field beam training method proposed in Ref. [40] effectively reduces the pilot overhead, revealing the nonlinear signal processing capacity of AI. Therefore, the AI-based method is perceived as a promising solution to the complex challenges in near-field communications. Specifically, it is reasonable to employ AI to deal with the massive parameters in near-field problems, such as beamforming and channel estimation.

In addition, most research mainly focuses on reducing the pilot overhead in the design of near-field beam training, while the effectiveness in complex environments is not fully explored. Hence, it is crucial to study the trade-off between low pilot overhead and high accuracy and propose an effective near-field beam training method that can be applied in complicated propagation environment with multiple mobile users and scatters.

4.2 XL-RIS-Aided Near-Field Localization

As derived in Ref. [56], the proposed algorithm with XL-RIS can achieve higher positioning resolution with proper design to utilize the richer AoA information. It is also possible for a single-RIS-aided system to provide a 3D localization function by exploiting the near-field channel model. Therefore, near-field XL-RIS-aided localization can be considered as a promising innovation, and it is valuable to carry out more studies in terms of theoretical error distribution analysis as well as practical positioning algorithms.

Although Ref. [56] has achieved great performance in XL-RIS-aided joint channel estimation and localization in a near-

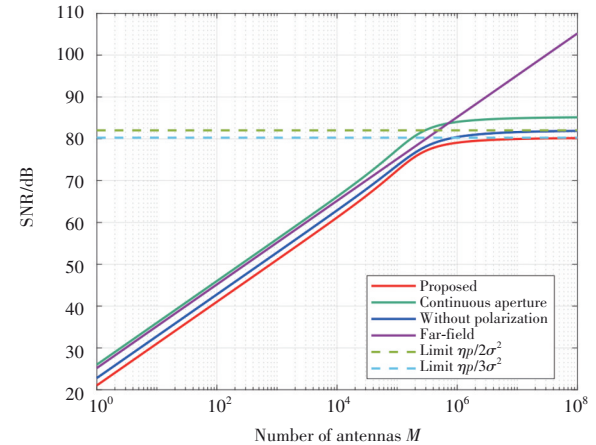

(a) SNR versus the number of antennas M

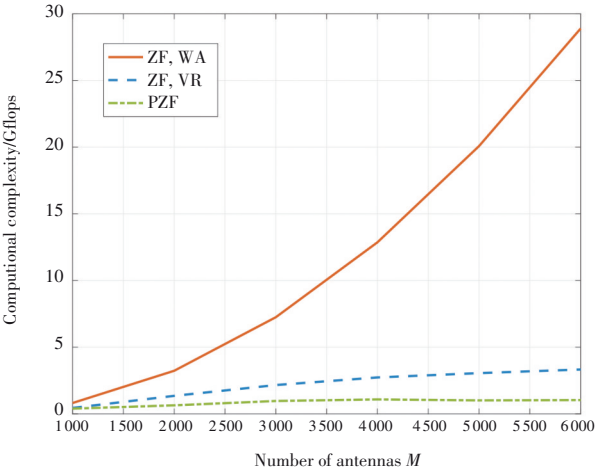

(b) Computational complexity versus the number of antennas M

PZF: partial zero-forcing VR: visibility region ZF: zero-forcing
SNR: signal-noise ratio WA: whole array

▲ **Figure 10. Effects of the number of antennas on system performance and computational complexity**

field scenario, the computational complexity is relatively high due to the massive elements. Therefore, it is valuable to design a near-field localization algorithm with low complexity and pilot overhead.

4.3 Near-Field Behavior of XL-Array

As one of the main innovations of 6G wireless communications, the successful application of XL-MIMO depends on the investigation and understanding of the near-field propagation. In addition, it is valuable to study the physically accurate near-field propagation model of XL-arrays.

Specifically, the near-field EM channel model proposed in Ref. [60] accurately depicts the physical EM wave transmission in the near-field scenario, which can be utilized to analyze the impact of discrete array aperture and polarization mismatch. Nevertheless, the physical channel model in Ref. [60] is totally based on theoretical analysis with Maxwell's EM field theory, so it is also meaningful to carry out channel measurements to verify and modify the near-field EM channel model.

Moreover, the authors in Ref. [58 – 60] utilized the information of VRs to remove the elements of the antenna array that contributed less to the signal transmission, and constructed equivalent dimensionality reduction channels to reduce the computational complexity. However, how to accurately measure VR using channel estimation methods is still an open question.

5 Conclusions

The far-field assumptions tend to be invalid owing to the large array size and short wavelength in 6G wireless communications. Hence, the near-field effect and spherical wavefront are no longer dispensable in some envisioned 6G scenarios. In this paper, we discussed the challenges and opportunities of near-field communication in terms of the fundamentals and applications in various schemes. We first introduced the three regions of free-space propagation and the corresponding wavefronts, with an emphasis on the radiating near-field and spherical wavefront. Then, we derived the near-field MIMO channel model and discussed the impact of spatial non-stationarity property on near-field propagation. In addition, we introduced several appealing works with respect to beam training and localization in the near-field scenarios and a recent work exploiting the spatial non-stationarity in the near field to achieve low-complexity transmission design. Finally, some insights into the future improvements of near-field communication were discussed.

References

[1] CHETTRI L, BERA R. A comprehensive survey on Internet of Things (IoT) toward 5G wireless systems [J]. IEEE Internet of Things journal, 2020, 7(1): 16 – 32. DOI: 10.1109/JIOT.2019.2948888
[2] GARCIA M H C, MOLINA-GALAN A, BOBAN M, et al. A tutorial on 5G NR V2X communications [J]. IEEE communications surveys & tutorials, 2021, 23(3): 1972 – 2026. DOI: 10.1109/COMST.2021.3057017
[3] LI S C, LI D X, ZHAO S S. 5G Internet of Things: a survey [J]. Journal of industrial information integration, 2018, 10: 1 – 9. DOI: 10.1016/j.jii.2018.01.005
[4] SHAFI M, MOLISCH A F, SMITH P J, et al. 5G: A tutorial overview of standards, trials, challenges, deployment, and practice [J]. IEEE journal on selected areas in communications, 2017, 35(6): 1201 – 1221. DOI: 10.1109/JSAC.2017.2692307
[5] SHAFIQUE K, KHAWAJA B A, SABIR F, et al. Internet of Things (IoT) for next-generation smart systems: A review of current challenges, future trends and prospects for emerging 5G-IoT scenarios [J]. IEEE access, 2020, 8: 23022 – 23040. DOI: 10.1109/ACCESS.2020.2970118
[6] WANG C X, HAIDER F, GAO X Q, et al. Cellular architecture and key technologies for 5G wireless communication networks [J]. IEEE communications magazine, 2014, 52(2): 122 – 130. DOI: 10.1109/MCOM.2014.6736752
[7] AGIWAL M, SAXENA N, ROY A. Towards connected living: 5G enabled Internet of Things (IoT) [J]. IETE technical review, 2019, 36(2): 190 – 202. DOI: 10.1080/02564602.2018.1444516
[8] YOU X H, WANG C X, HUANG J, et al. Towards 6G wireless communication networks: vision, enabling technologies, and new paradigm shifts [J]. Science China information sciences, 2020, 64(1): 110301. DOI: 10.1007/s11432-020-2955-6
[9] ZHANG Z Q, XIAO Y, MA Z, et al. 6G wireless networks: vision, requirements, architecture, and key technologies [J]. IEEE vehicular technology magazine, 2019, 14(3): 28 – 41. DOI: 10.1109/MVT.2019.2921208
[10] YANG P, XIAO Y, XIAO M, et al. 6G wireless communications: vision and potential techniques [J]. IEEE network, 2019, 33(4): 70 – 75. DOI: 10.1109/MNET.2019.1800418
[11] ZHANG L, LIANG Y C, NIYATO D. 6G Visions: Mobile ultra-broadband, super internet-of-things, and artificial intelligence [J]. China communications, 2019, 16(8): 1 – 14. DOI: 10.23919/JCC.2019.08.001
[12] LU H Q, ZENG Y, YOU C S, et al. A tutorial on near-field XL-MIMO communications towards 6G [EB/OL]. (2023-10-17) [2023-11-10]. http://arxiv.org/abs/2310.11044
[13] PIZZO A, SANGUINETTI L, MARZETTA T L. Fourier plane-wave series expansion for holographic MIMO communications [J]. IEEE transactions on wireless communications, 2022, 21(9): 6890 – 6905. DOI: 10.1109/TWC.2022.3152965
[14] CUI M Y, WU Z D, LU Y, et al. Near-field MIMO communications for 6G: Fundamentals, challenges, potentials, and future directions [J]. IEEE communications magazine, 2023, 61(1): 40 – 46. DOI: 10.1109/MCOM.004.2200136
[15] TATARIA H, SHAFI M, MOLISCH A F, et al. 6G wireless systems: Vision, requirements, challenges, insights, and opportunities [J]. Proceedings of the IEEE, 2021, 109(7): 1166 – 1199. DOI: 10.1109/JPROC.2021.3061701
[16] AN J C, YUEN C, DAI L L, et al. Toward beam focusing-aided near-field communications: research advances, potential, and challenges [EB/OL] (2023-09-17) [2023-11-10]. http://arxiv.org/abs/2309.09242
[17] LIU Y W, WANG Z L, XU J Q, et al. Near-field communications: a tutorial review [EB/OL]. [2023-11-10]. http://arxiv.org/abs/2305.17751.pdf
[18] ZHANG H Y, SHLEZINGER N, GUIDI F, et al. 6G wireless communications: from far-field beam steering to near-field beam focusing [J]. IEEE communications magazine, 2023, 61(4): 72 – 77. DOI: 10.1109/MCOM.001.2200259
[19] SHERMAN J. Properties of focused apertures in the Fresnel region [J]. IRE transactions on antennas and propagation, 1962, 10(4): 399 – 408.

DOI: 10.1109/TAP.1962.1137900
[20] SELVAN K T, JANASWAMY R. Fraunhofer and Fresnel Distances: unified derivation for aperture antennas [J]. IEEE antennas and propagation magazine, 2017, 59(4): 12 – 15. DOI: 10.1109/MAP.2017.2706648
[21] KRAUS J D, MARHEFKA R J. Antennas for all applications [M]. New York, USA: McGraw-Hill School, 2001
[22] LU H Q, ZENG Y. Communicating with extremely large-scale array/surface: unified modeling and performance analysis [J]. IEEE transactions on wireless communications, 2022, 21(6): 4039 – 4053. DOI: 10.1109/TWC.2021.3126384
[23] HEATH R W, GONZÁLEZ-PRELCIC N, RANGAN S, et al. An overview of signal processing techniques for millimeter wave MIMO systems [J]. IEEE journal of selected topics in signal processing, 2016, 10(3): 436 – 453. DOI: 10.1109/JSTSP.2016.2523924
[24] CUI M Y, DAI L L. Channel estimation for extremely large-scale MIMO: far-field or near-field? [J]. IEEE transactions on communications, 2022, 70(4): 2663 – 2677. DOI: 10.1109/TCOMM.2022.3146400
[25] MARTÍNEZ À O, DE CARVALHO E, NIELSEN J Ø. Towards very large aperture massive MIMO: a measurement based study [C]//IEEE Globecom Workshops (GC Wkshps). IEEE, 2014: 281 – 286. DOI: 10.1109/GLOCOMW.2014.7063445
[26] YUAN Z Q, ZHANG J H, JI Y L, et al. Spatial non-stationary near-field channel modeling and validation for massive MIMO systems [J]. IEEE transactions on antennas and propagation, 2023, 71(1): 921 – 933. DOI: 10.1109/TAP.2022.3218759
[27] HAN Y, JIN S, WEN C K, et al. Channel estimation for extremely large-scale massive MIMO systems [J]. IEEE wireless communications letters, 2020, 9(5): 633 – 637. DOI: 10.1109/LWC.2019.2963877
[28] TIAN J C, HAN Y, JIN S, et al. Low-overhead localization and VR identification for subarray-based ELAA systems [J]. IEEE wireless communications letters, 2023, 12(5): 784 – 788. DOI: 10.1109/LWC.2023.3244000
[29] LÓPEZ C F, WANG C X. Novel 3-D non-stationary wideband models for massive MIMO channels [J]. IEEE transactions on wireless communications, 2018, 17(5): 2893 – 2905. DOI: 10.1109/TWC.2018.2804385
[30] WANG J, WANG C X, HUANG J, et al. A general 3D space-time-frequency non-stationary THz channel model for 6G ultra-massive MIMO wireless communication systems [J]. IEEE journal on selected areas in communications, 2021, 39(6): 1576 – 1589. DOI: 10.1109/JSAC.2021.3071850
[31] BAI T Y, HEATH R W. Analysis of beam sweep channel estimation in MmWave massive MIMO networks [C]//IEEE Global Conference on Signal and Information Processing (GlobalSIP). IEEE, 2016: 615 – 619. DOI: 10.1109/GlobalSIP.2016.7905915
[32] CHEN K J, QI C H, LI G Y. Two-step codeword design for millimeter wave massive MIMO systems with quantized phase shifters [J]. IEEE transactions on signal processing, 1027, 68: 170 – 180. DOI: 10.1109/TSP.2019.2959250
[33] MA K, HE D X, SUN H C, et al. Deep learning assisted mmWave beam prediction with prior low-frequency information [C]//IEEE International Conference on Communications. IEEE, 2021: 1 – 6. DOI: 10.1109/ICC42927.2021.9500788
[34] QI C H, WANG Y J, LI G Y. Deep learning for beam training in millimeter wave massive MIMO systems [J]. IEEE transactions on wireless communications, 2020. DOI: 10.1109/TWC.2020.3024279
[35] QI C H, DONG P H, MA W Y, et al. Acquisition of channel state information for mmWave massive MIMO: traditional and machine learning-based approaches [J]. Science China information sciences, 2021, 64(8): 181301. DOI: 10.1007/s11432-021-3247-2
[36] WEI X H, DAI L L, ZHAO Y J, et al. Codebook design and beam training for extremely large-scale RIS: far-field or near-field? [J]. China communications, 2022, 19(6): 193 – 204. DOI: 10.23919/JCC.2022.06.015
[37] ZHANG Y P, WU X, YOU C S. Fast near-field beam training for extremely large-scale array [J]. IEEE wireless communications letters, 2022, 11(12): 2625 – 2629. DOI: 10.1109/LWC.2022.3212344
[38] REZAIE S, MANCHÓN C N, DE CARVALHO E. Location- and orientation-aided millimeter wave beam selection using deep learning [C]//IEEE International Conference on Communications (ICC). IEEE, 2020: 1 – 6. DOI: 10.1109/ICC40277.2020.9149272
[39] JIANG G L, QI C H. Near-field beam training based on deep learning for extremely large-scale MIMO [J]. IEEE communications letters, 2023, 27(8): 2063 – 2067. DOI: 10.1109/LCOMM.2023.3289513
[40] LIU W, REN H, PAN C H, et al. Deep learning based beam training for extremely large-scale massive MIMO in near-field domain [J]. IEEE communications letters, 2023, 27(1): 170 – 174. DOI: 10.1109/LCOMM.2022.3210042
[41] LIU W, PAN C H, REN H, et al. Low-overhead beam training scheme for extremely large-scale RIS in near field [J]. IEEE transactions on communications, 2023, 71(8): 4924 – 4940. DOI: 10.1109/TCOMM.2023.3278728
[42] FAN D, GAO F F, LIU Y W, et al. Angle domain channel estimation in hybrid millimeter wave massive MIMO systems [J]. IEEE transactions on wireless communications, 2018, 17(12): 8165 – 8179. DOI: 10.1109/TWC.2018.2874640
[43] ZHOU G, PAN C H, REN H, et al. Channel estimation for RIS-aided multiuser millimeter-wave systems [J]. IEEE transactions on signal processing, 2021, 70: 1478 – 1492. DOI: 10.1109/TSP.2022.3158024
[44] HE J G, WYMEERSCH H, KONG L, et al. Large intelligent surface for positioning in millimeter wave MIMO systems [C]//The 91st Vehicular Technology Conference (VTC2020-Spring). IEEE, 2020: 1 – 5. DOI: 10.1109/VTC2020-Spring48590.2020.9129075
[45] LIU Y, HONG S, PAN C H, et al. Optimization of RIS configurations for multiple-RIS-aided mmWave positioning systems based on CRLB analysis [EB/OL]. (2021-11-28) [2023-12-12]. http://arxiv.org/abs/2111.14023
[46] WANG R, XING Z, LIU E W. Joint location and communication study for intelligent reflecting surface aided wireless communication system [EB/OL]. (2021-05-01) [2023-12-12]. http://arxiv.org/abs/2103.01063
[47] FENG Z Y, WANG B, ZHAO Y P, et al. Power optimization for target localization with reconfigurable intelligent surfaces [J]. Signal processing, 2021, 189: 108252. DOI: 10.1016/j.sigpro.2021.108252
[48] ELZANATY A, GUERRA A, GUIDI F, et al. Reconfigurable intelligent surfaces for localization: position and orientation error bounds [J]. IEEE transactions on signal processing, 2021, 69: 5386 – 5402. DOI: 10.1109/TSP.2021.3101644
[49] ZHANG H B, ZHANG H L, DI B Y, et al. Towards ubiquitous positioning by leveraging reconfigurable intelligent surface [J]. IEEE communications letters, 2021, 25(1): 284 – 288. DOI: 10.1109/LCOMM.2020.3023130
[50] HE J G, WYMEERSCH H, SANGUANPUAK T, et al. Adaptive beamforming design for mmWave RIS-aided joint localization and communication [C]//IEEE Wireless Communications and Networking Conference Workshops (WCNCW). IEEE, 2020: 1 – 6. DOI: 10.1109/WCNCW48565.2020.9124848
[51] FASCISTA A, COLUCCIA A, WYMEERSCH H, et al. RIS-aided joint localization and synchronization with a single-antenna mmwave receiver

[C]//IEEE International Conference on Acoustics, Speech and Signal Processing (ICASSP). IEEE, 2021: 4455 – 4459. DOI: 10.1109/ICASSP39728.2021.9413515

[52] WU T, PAN C H, PAN Y J, et al. Fingerprint-based mmWave positioning system aided by reconfigurable intelligent surface [J]. IEEE wireless communications letters, 2023, 12(8): 1379 – 1383. DOI: 10.1109/LWC.2023.3275204

[53] CHEN J C, HUDSON R E, YAO K. Maximum-likelihood source localization and unknown sensor location estimation for wideband signals in the near-field [J]. IEEE transactions on signal processing, 2002, 50(8): 1843 – 1854. DOI: 10.1109/TSP.2002.800420

[54] ABU-SHABAN Z, KEYKHOSRAVI K, KESKIN M F, et al. Near-field localization with a reconfigurable intelligent surface acting as lens [C]//IEEE International Conference on Communications. IEEE, 2021: 1 – 6. DOI: 10.1109/ICC42927.2021.9500663

[55] RAHAL M, DENIS B, KEYKHOSRAVI K, et al. RIS-enabled localization continuity under near-field conditions [C]//The 22nd International Workshop on Signal Processing Advances in Wireless Communications (SPAWC). IEEE, 2021: 436 – 440. DOI: 10.1109/SPAWC51858.2021.9593200

[56] PAN Y J, PAN C H, JIN S, et al. RIS-aided near-field localization and channel estimation for the terahertz system [J]. IEEE journal of selected topics in signal processing, 2023, 17(4): 878 – 892. DOI: 10.1109/JSTSP.2023.3285431

[57] PAYAMI S, TUFVESSON F. Channel measurements and analysis for very large array systems at 2.6 GHz [C]//The 6th European Conference on Antennas and Propagation (EUCAP). IEEE, 2012: 433 – 437. DOI: 10.1109/EuCAP.2012.6206345

[58] AMIRI A, ANGJELICHINOSKI M, DE CARVALHO E, et al. Extremely large aperture massive MIMO: low complexity receiver architectures [C]//IEEE Globecom Workshops (GC Wkshps). IEEE, 2018: 1 – 6. DOI: 10.1109/GLOCOMW.2018.8644126

[59] MARINELLO J C, ABRÃO T, AMIRI A, et al. Antenna selection for improving energy efficiency in XL-MIMO systems [J]. IEEE transactions on vehicular technology, 2020, 69(11): 13305 – 13318. DOI: 10.1109/TVT.2020.3022708

[60] ZHI K D, PAN C H, REN H, et al. Performance analysis and low-complexity design for XL-MIMO with near-field spatial non-stationarities [EB/OL]. (2023-03-21) [2023-12-12]. http://arxiv.org/abs/2304.00172

Biographies

LIU Mengyu received his BE degree from the School of Electronic and Information Engineering, Beijing Jiaotong University, China in 2023. He is currently pursuing his ME degree with the School of Information Science and Engineering, Southeast University, China. His research interests include massive MIMO, reconfigurable intelligent surfaces (RIS), and near-field communications.

ZHANG Yang received his BE degree from the Harbin Institute of Technology, China in 2023. He is currently pursuing his ME degree with the School of Information Science and Engineering, Southeast University, China. His research interests include reconfigurable intelligent surfaces (RIS), array signal processing, near-field communications, and localization.

JIN Yasheng received his BE degree from the Bell Honors School, Nanjing University of Posts and Telecommunications, China in 2023. He is currently pursuing his ME degree with the School of Information Science and Engineering, Southeast University, China. His research interests include massive MIMO, reconfigurable intelligent surfaces (RIS), machine learning and near-field communications.

ZHI Kangda received his BE degree from the School of Communication and Information Engineering, Shanghai University, China in 2017, ME degree from School of Information Science and Technology, University of Science and Technology of China in 2020, and PhD degree from the School of Electronic Engineering and Computer Science, Queen Mary University of London, UK in 2023. His research interests include reconfigurable intelligent surface (RIS), massive MIMO, and near-field communications. He received the Exemplary Reviewer Certificate of the IEEE Wireless Communications Letters in 2021 and 2022.

PAN Cunhua (cpan@seu.edu.cn) received his BS and PhD degrees from the School of Information Science and Engineering, Southeast University, China in 2010 and 2015, respectively. From 2015 to 2016, he was a research associate at the University of Kent, UK. He held a post-doctoral researcher position at the Queen Mary University of London, UK from 2016 to 2019, where he was a lecturer from 2019 to 2021. Since 2021, he has been a full professor with Southeast University. His research interests include reconfigurable intelligent surfaces (RIS), intelligent reflection surface (IRS), ultra-reliable low latency communication (URLLC), machine learning, UAV, the Internet of Things, and mobile edge computing. He has published over 120 IEEE journal articles. He received the IEEE ComSoc Leonard G. Abraham Prize and IEEE ComSoc Asia-Pacific Outstanding Young Researcher Award both in 2022.